ADVANCED MATERIALS
www.advmat.de

Chemically Exfoliated VSe_2 Monolayers with Room-Temperature Ferromagnetism

*Wei Yu, Jing Li, Tun Seng Herng, Zishen Wang, Xiaoxu Zhao, Xiao Chi, Wei Fu, Ibrahim Abdelwahab, Jun Zhou, Jiadong Dan, Zhongxin Chen, Zhi Chen, Zejun Li, Jiong Lu, Stephen J. Pennycook, Yuan Ping Feng, Jun Ding, and Kian Ping Loh**

Among van der Waals layered ferromagnets, monolayer vanadium diselenide (VSe_2) stands out due to its robust ferromagnetism. However, the exfoliation of monolayer VSe_2 is challenging, not least because the monolayer flake is extremely unstable in air. Using an electrochemical exfoliation approach with organic cations as the intercalants, monolayer 1T-VSe_2 flakes are successfully obtained from the bulk crystal at high yield. Thiol molecules are further introduced onto the VSe_2 surface to passivate the exfoliated flakes, which improves the air stability of the flakes for subsequent characterizations. Room-temperature ferromagnetism is confirmed on the exfoliated 2D VSe_2 flakes using a superconducting quantum interference device (SQUID), X-ray magnetic circular dichroism (XMCD), and magnetic force microscopy (MFM), where the monolayer flake displays the strongest ferromagnetic properties. Se vacancies, which can be ubiquitous in such materials, also contribute to the ferromagnetism of VSe_2, although density functional theory (DFT) calculations show that such effect can be minimized by physisorbed oxygen molecules or covalently bound thiol molecules.

2D intrinsic ferromagnets with high Curie temperature (T_c) are desirable for spintronic applications. The atomic thickness of van der Waals (vdW) crystals allow magnetic ordering to be electrically controlled, which is useful in memory applications.[1–3] At the fundamental level, ferromagnetic ordering at the 2D limit is a fascinating topic because long range magnetic order is predicted to be suppressed at finite temperature according to the Mermin–Wagner theorem, however, recent discoveries prove that there are exceptions.[4] For instance, atomically thin CrI_3 and $Cr_2Ge_2Te_6$, were discovered as intrinsic ferromagnets by Xu et al. and Zhang et al., respectively.[5,6] This stimulates the search for other members in this 2D ferromagnets family, which is soon joined by Fe_3GeTe_2 and VSe_2.[7,8] Among them, monolayer VSe_2 (1T and 2H phase) is notable for its high T_c, due to the strong electron coupling in $3d^1$ odd-electronic configuration of V^{4+}.[9–13] Besides ferromagnetism, enhanced charge density wave (CDW) transition temperature, metal–insulator transition, and valley polarization have been demonstrated or predicted to exist in monolayer VSe_2 as well.[14–16] Recently, single-layer 1T-VSe_2 was successfully grown by Batzill et al. using molecular beam epitaxy (MBE) on vdW substrate including highly-oriented pyrolytic graphite (HOPG) and MoS_2 and its robust room-temperature ferromagnetism was confirmed by magnetic measurements.[8]

The origin of the ferromagnetism in monolayer VSe_2 is still under debate, some theoretician has questioned if the ferromagnetism is intrinsic in nature since calculations suggest that CDW distortion can remove the intrinsic ferromagnetic ground state in VSe_2.[17] Moreover, recent angle-resolved photoemission (ARPES) studies on MBE grown monolayer VSe_2 revealed the absence of ferromagnetic order as no exchange splitting was observed.[15,18,19] These MBE grown VSe_2 samples were grown on polycrystalline HOPG substrate, thus the films are coalesced from micrometer-sized domains and contain a lot of grain boundaries and misoriented domains, which would induce spin frustration. It is challenging to verify ferromagnetism in single crystalline VSe_2 due to the difficulty to isolate monolayer flake by micromechanical exfoliation; the theoretical interlayer distance of 1T-VSe_2 (0.61 nm), as illustrated in **Figure 1**a, is

---

W. Yu, Dr. J. Li, Dr. X. Chi, Dr. W. Fu, I. Abdelwahab, Dr. Z. X. Chen,
Dr. Z. Chen, Dr. Z. Li, Prof. J. Lu, Prof. K. P. Loh
Department of Chemistry
National University of Singapore
3 Science Drive 3, Singapore 117543, Singapore
E-mail: chmlohkp@nus.edu.sg

Dr. J. Li, Z. Wang, Dr. W. Fu, I. Abdelwahab, Dr. Z. Li, Prof. J. Lu,
Prof. Y. P. Feng, Prof. K. P. Loh
Centre for Advanced 2D Materials and Graphene Research Centre
National University of Singapore
Singapore 117546, Singapore

Dr. T. S. Herng, Dr. X. Zhao, J. Dan, Prof. S. J. Pennycook, Prof. J. Ding
Department of Materials Science and Engineering
National University of Singapore
9 Engineering Drive 1, Singapore 117575, Singapore

Z. Wang, Dr. J. Zhou, Prof. Y. P. Feng
Department of Physics
National University of Singapore
2 Science Drive 3, Singapore 117551, Singapore

Dr. X. Chi
Singapore Synchrotron Light Source
National University of Singapore
5 Research Link, Singapore 117603, Singapore

The ORCID identification number(s) for the author(s) of this article can be found under https://doi.org/10.1002/adma.201903779.

DOI: 10.1002/adma.201903779

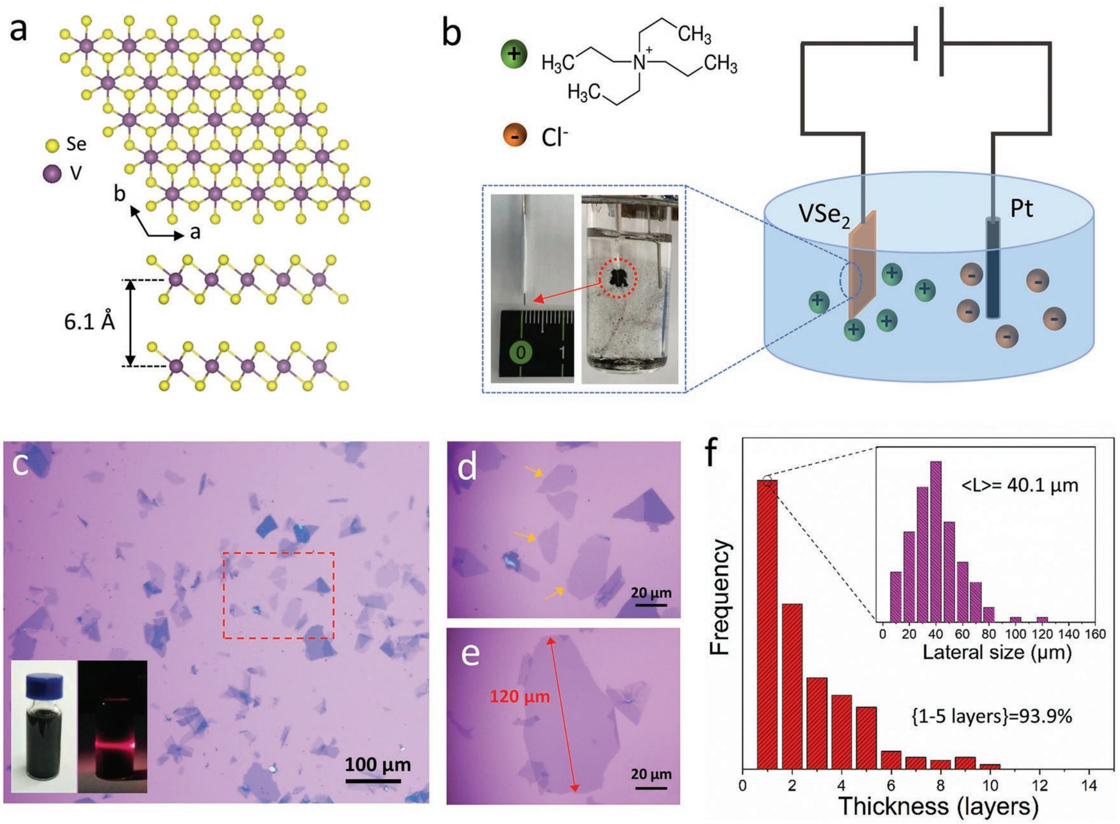

Figure 1. Illustration of the electrochemical exfoliation of 1T-VSe_2. a) Top and side view of the atomic structure of layered 1T-VSe_2 crystal ($a = b = 3.35$ Å, $c = 6.1$ Å). b) Schematic illustration of the electrochemical setup for cathode exfoliation of VSe_2 using tetrapropylammonium cation (TPA) as the intercalant. Inset: photograph showing a small piece of VSe_2 crystal clamped by two titanium plates (left), visible expansion of VSe_2 cathode with a fluffy shape (right). c–e) OM images of drop-casted ultrathin VSe_2 flakes on SiO_2 substrates. Inset: VSe_2 dispersion solution after manual shaking (left) and its strong Tyndall effect (right). d) Zoomed-in OM images of the red dashed square in (d). e) Large-sized VSe_2 monolayer flake up to 120 µm. f) Statistical histograms for the thickness distributions of exfoliated ultrathin VSe_2 flakes and (inset histogram) lateral size distributions of VSe_2 monolayers.

narrower than MoS_2 (0.65 nm).[14] Another more challenging problem is that monolayer VSe_2 is prone to oxidation and any ferromagnetism would vanish quickly. One way around this may be to use solution phase exfoliation methods to produce monolayer flake and passivate it immediately in situ in solution. Motivated by recent successful electrochemical exfoliation of 2D black phosphorous using organic ammonium cations as the intercalants, we performed organic-solvent based electrochemical exfoliation of 1T-VSe_2 in this work.[20–22] The results show that large sized ultrathin VSe_2 flakes with well-defined thickness and size distribution could be obtained, and passivated from air oxidation by thiol molecules. Magnetic measurements were performed to verify room-temperature ferromagnetism of these exfoliated ultrathin VSe_2 flakes.

The ambient two-electrode electrochemical setup using for the cathode exfoliation of VSe_2 crystal is illustrated in Figure 1b. An organic quaternary ammonium salt with four C_3 alkyl chains, tetrapropylammonium (TPA) chloride, was selected as the intercalants for exfoliation. Compared to traditional metal ions (Li^+, Na^+), TPA does not introduce significant charges into the host structure, and its large size provides higher expansion efficiency of the crystal once it is intercalated. The electrolyte solvent we used is propylene carbonate (PC), a polar organic solvent with high boiling point (242 °C), in which VSe_2 nanosheets can be dispersed well. Meanwhile, this high boiling point solvent also acts as a protection barrier for the unstable ultrathin VSe_2 flakes, such that the electrochemical exfoliation can be performed in air. After electrochemical intercalation, manual shaking of the expanded crystal yielded VSe_2 dispersion (Figure 1d, inset) with a large percentage (93.9%) of micrometer-sized, ultrathin flakes (one to five layers). To facilitate manual-shaking exfoliation, the working voltage and concentration of electrolyte have to be optimized to yield a cotton-like shape of expanded VSe_2 crystal, as can be seen in the inset in Figure 1b (see the Supporting Information). The VSe_2 dispersion shows a strong Tyndall effect, indicating the uniform dispersion of ultrathin flakes of VSe_2 in PC (Figure 1d, inset). Figure 1c–e shows the optical microscopy (OM) images of the drop-casted VSe_2 flakes on SiO_2-coated silicon substrate, where majority of them are ultrathin flakes and lateral size of monolayer is up to 120 µm. Figure 1f presents the statistical histograms of the thickness and monolayer size of exfoliated VSe_2, as determined using OM, atomic force microscopy (AFM) and transmission electron microscopy (TEM). More than 90% of the VSe_2 flakes are between one and five layers with an average lateral size of ≈40 µm. Therefore, we can conclude that electrochemical exfoliation method is more effective than micromechanical exfoliation methods in generating large sized, monolayer VSe_2 flake with a much higher yield.

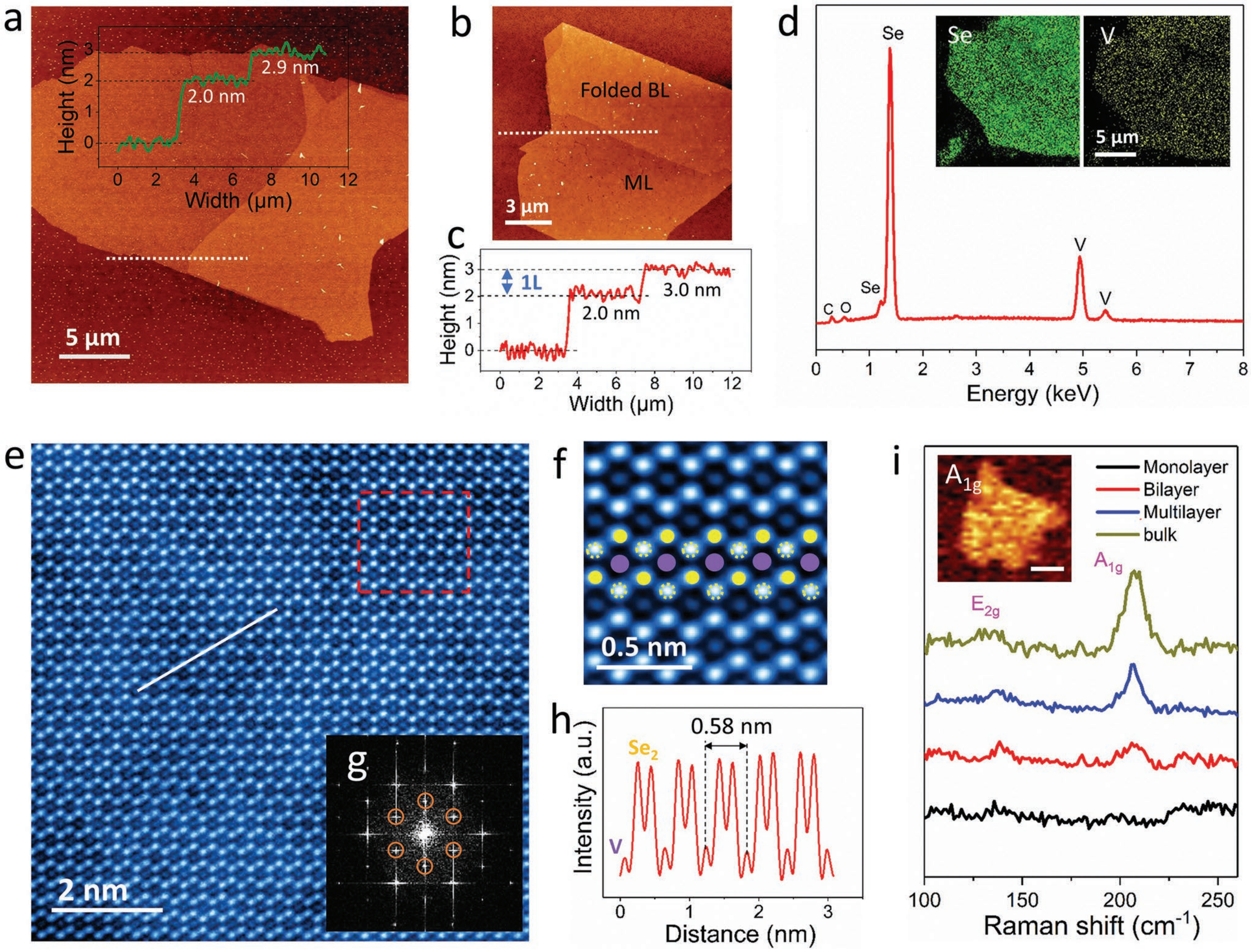

Figure 2. Structural characterizations of exfoliated VSe_2 flakes. AFM topography images of a) stepped and b) folded monolayer/bilayer VSe_2 flakes with height profile along the dashed line in (a). c) AFM height profile along the dashed line in (b) indicating the real single-layer thickness. d) EDS elemental analysis of exfoliated VSe_2 flake. Inset: V-K edge and Se-L edge mapping images. e) Atomic-resolution STEM image of exfoliated VSe_2 flake. f) Zoomed-in atomic image of the region highlighted by the red dashed square in (e). Purple circled V atoms, yellow circled Se atoms (bottom Se in dashed). g) Fast Fourier transform (FFT) pattern of the VSe_2 flake. h) Intensity line profile along the white line in (e) showing the in-plane lattice constant a. i) Layer-dependent Raman spectra of VSe_2 from monolayer to bulk. Inset: Raman mapping image on A_{1g} modes of a few-layer VSe_2 flake.

To analyze the morphology of the exfoliated VSe_2 monolayers, AFM and scanning transmission electron microscopy (STEM) were performed. A clean flake with step heights of 2.0 and 2.9 nm is shown in the AFM image in **Figure 2**a, these are attributed to monolayer and bilayer thick VSe_2, respectively. In fact, the theoretical interlayer distance of each atomic layer is 0.61 nm, the much larger heights are due to organic residues and substrate effects, which has also been found in other liquid exfoliated samples.[23] To prove that this is the case, a folded edge in a monolayer sample was measured by AFM (Figure 2b). From the height profile, we can clearly see that the top folded layer has a thickness of 1.0 ± 0.1 nm while the bottom layer is 2.0 nm thick, suggesting that trapped solvent can give an error margin of 1 nm to the thickness (Figure 2c). Monolayer VSe_2 has also been examined by atomic-resolution STEM as shown in Figure S1 (Supporting Information), showing Se vacancies. Energy dispersive X-ray spectroscopic (EDS) analysis of the exfoliated few-layer VSe_2 flake indicates its high purity (Figure 2d). The chemical stoichiometry of exfoliated VSe_2 has been verified as V:Se = 1:1.84 ± 0.02 by X-ray photoelectron spectroscopy (XPS) spectra (Figure S2a, Supporting Information), which has also been confirmed by TEM quantitative analysis for Se vacancy concentrations of monolayer (≈11.0%) and bilayer flakes (≈12.2%).

To study the atomic structure of the exfoliated VSe_2, high-resolution TEM was performed. As shown in Figure 2e,f, atomic-resolution STEM image of a few-layer VSe_2 flake reveals the octahedral 1T phase. Fast Fourier transform (FFT) pattern of the flake shows a sixfold rotational symmetric diffraction, due to the single-crystalline hexagonal structure (Figure 2g). The in-plane lattice constant a is revealed to be 3.35 ± 0.01 Å ($0.58/\sqrt{3}$), which agrees well with the documented constant of 1T-VSe_2 (Figure 2h).[24] To confirm the structure and crystallinity of the exfoliated VSe_2, Raman spectra and mapping were studied as shown in Figure 2i. For 1T-VSe_2, the in-plane E_{2g} and out-of-plane A_{1g} vibration peaks occur at 135 and 206 cm^{-1},

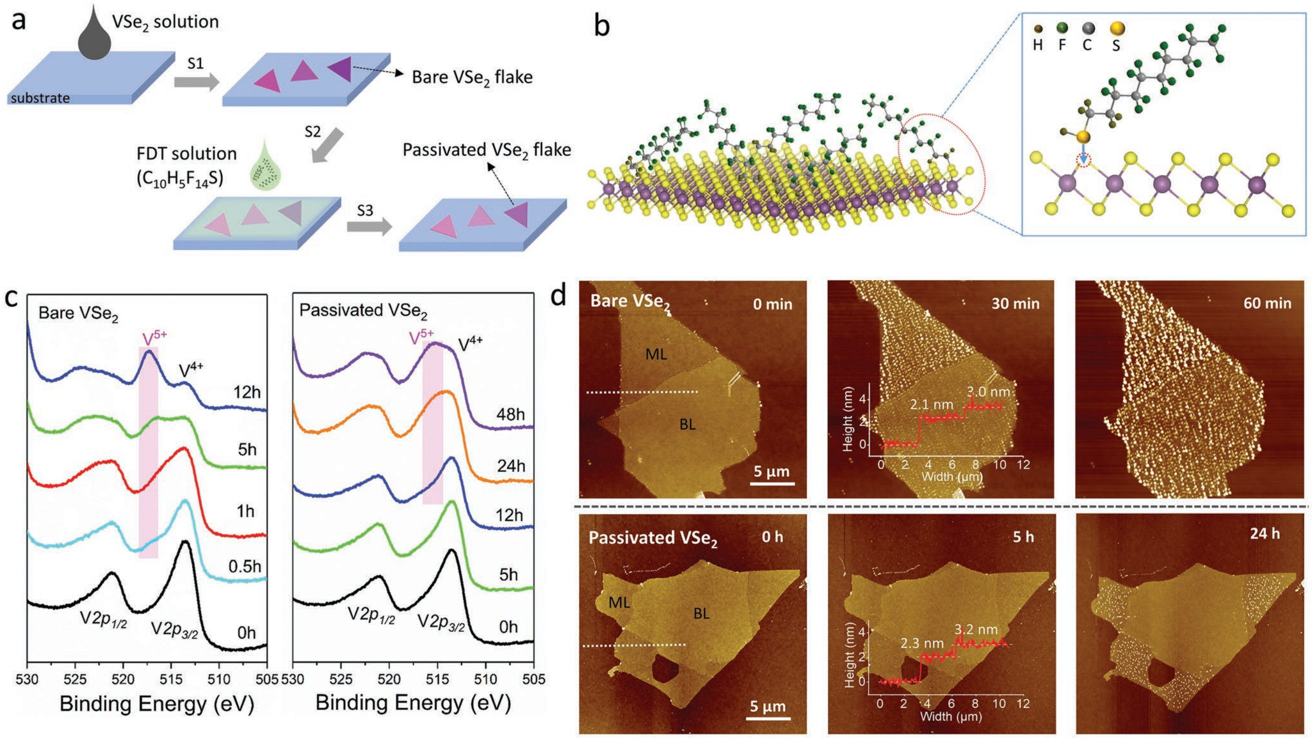

Figure 3. Covalent passivation of exfoliated VSe$_2$ flakes. a) Schematic illustration of the covalent passivation processes (S1–S3) on exfoliated VSe$_2$ flakes. S1, Drop-casting VSe$_2$ dispersion on a SiO$_2$ substrate and vacuum drying; S2, Capping the VSe$_2$/SiO$_2$ substrate by pure organic FDT solution; S3, Removing FDT solution and washing with acetone. b) Schematic illustration for the covalent passivation mechanism bonding on Se defects by the thiol group. c) XPS V2p spectra of bare and passivated VSe$_2$ flakes on HOPG substrate after ambient exposures for different lengths of time. d) AFM topography images of bare and passivated monolayer/bilayer VSe$_2$ flakes after ambient exposure for different lengths of time. Top: bare VSe$_2$, 0–60 min; Bottom: passivated VSe$_2$, 0–24 h. Inset (middle images): AFM height profiles of the bare and passivated VSe$_2$ flakes corresponding to the white dashed lines in left image.

respectively.[25] The Raman spectrum of bulk VSe$_2$ crystal agrees very well with that of 1T phase with two intensive peaks at 135.8 and 207.0 cm^{-1}, and a good phase retention is observed from bulk to monolayer. However, it was observed that monolayer VSe$_2$ flake is easily damaged by laser irradiation, and the Raman peaks decrease in intensity with laser irradiation time. We had verified that flake is highly prone to laser damage by monitoring the rapidly laser-induced amorphization of monolayer VSe$_2$ using STEM (Figure S3, Supporting Information). Bilayer VSe$_2$ is much more stable than monolayer ones and exhibits obvious Raman peaks. For typical 2D materials, the ratio of A$_{1g}$/E$_{2g}$ is related to the layer thickness and different degrees of interlayer coupling.[26] From bulk to bilayer VSe$_2$, the A$_{1g}$/E$_{2g}$ intensity ratio is dramatically decreased from 3.77 to 1.05. The peak intensity map of the out-of-plane A$_{1g}$ mode on a bilayer VSe$_2$ flake in Figure 2i (inset) indicating a homogenous thickness and uniform 1T structure with high crystallinity.

Similar to what was observed previously, we find that 2D VSe$_2$ is extremely unstable in air and easily oxidized to form vanadium oxides (V$_2$O$_5$). XPS results of the exfoliated VSe$_2$ ultrathin nanosheets reveal that the Se/V stoichiometry ratio is around 1.84, suggesting the presence of Se vacancies, which may be the origin of the air instability as metallic atoms with unpaired electrons are prone to oxidation. One way of passivating defects due to Se vacancies is to covalently bind thiol molecules to the V-atoms at the Se-vacancies, for this we introduced 1H, 1H, 2H, 2H-perfluorodecanethiol (FDT) to passivate the exfoliated VSe$_2$ flakes.[27–29] The choice of FDT was also motivated by the presence of hydrophobic fluorine groups in the molecular chain, which can serve as a barrier to moisture permeation. The procedure for the covalent passivation of the exfoliated VSe$_2$ is illustrated in **Figure 3**a. FDT solution was introduced onto the surface of the sample to fully cover it for 1 d, followed by washing with acetone to remove the physically adsorbed molecules. All steps were performed in a glove box to avoid the degradation of VSe$_2$ during the passivation period. After this treatment, FDT molecules were found to be anchored on VSe$_2$ surface by covalent bond. The XPS F1s and S3s spectra in Figure S4a,b (Supporting Information) show strong F and weak S signals indicating the formation of a FDT adlayer on the sample surface. To exclude the possibility of physically adsorbed molecules, XPS was used to monitor the F1s after annealing the sample in ultrahigh vacuum (UHV, pressure $<5 \times 10^{-10}$ mbar) above the boiling point of FDT (355 K atm^{-1}). As shown in Figure S4c (Supporting Information), after annealing at 400 K in UHV for 1 h (return to base pressure), the intensity of F1s peak was only slightly decreased. When the annealing temperature was increased to 500 K, the F1s peak is dramatically weakened, and it disappears after annealing at 600 K for 1 h. These results proved the formation of strong chemical bonds between FDT and VSe$_2$, as illustrated in Figure 3b.

To evaluate the effectiveness of this passivation method against air-induced degradation, OM, XPS, and AFM topography were used to investigate the chemical state and morphology of the VSe_2 flakes. From the OM images in Figure S5 (Supporting Information), we can see that the color contrast of the as-exfoliated VSe_2 (bare VSe_2) monolayer becomes lighter after 30 min of air exposure, whereas this change occurs more slowly on bare bilayer VSe_2. In contrast, both monolayer and bilayer FDT-passivated VSe_2 (Passivated VSe_2) flakes show almost no color change up to 5 h, and bilayer flake exhibits slight color change only after 24 h. The oxidative degradation of VSe_2 to VO_x species causes the flake to be increasingly transparent, this is confirmed by V2p XPS spectra (Figure 3c), which shows that the valence state of vanadium is increased from V^{4+} to V^{5+} as judged by the +3.7 eV chemical shift of the $V2p_{3/2}$ peak. The V2p spectra of the passivated VSe_2 sample after 5 h of air exposure are almost the same with initial one. After 12 h of air exposure, the proportions of the oxidized V^{5+} ($2p_{3/2}$ orbital electrons), as seen from the deconvoluted XPS spectra for the bare and passivated VSe_2, are 67.4% and 13.2%, respectively (Figure S6a, Supporting Information). Thus, XPS data corroborate the evidence shown by the optical images regarding the improved air-stability of the FDT-passivated VSe_2 flakes. Following air exposure, AFM study on both bare and passivated VSe_2 monolayer/bilayer flakes was also performed, as shown in Figure 3d. The inserted height profiles show the thicknesses of both monolayer and bilayer as we discussed above (≈2.0 and 3.0 nm, respectively). The thickness of the passivated monolayer flake is slightly larger than the bare one by around 0.2 nm, and this height difference is due to the anchored FDT molecules on VSe_2 basal plane. Degradation of the samples can be judged from the formation of particles on the surface. For bare VSe_2 sample, the monolayer is severely degraded after 30 min, whereas the bilayer flake is fully degraded after 1 h (Figure 3d, top). For the passivated VSe_2 sample, monolayer appears unchanged from the initial sample after 5 h, and only slight surface degradation occurs in the bilayer flake after 24 h of air exposure (Figure 3d, bottom). Therefore, AFM results confirmed effective passivation on both monolayer and bilayer VSe_2.

Ultrathin VSe_2 flakes, scattered on SiO_2 substrate, were analyzed for its magnetic properties by collecting the magnetization-magnetic field (*M*–*H*) curves on a superconducting quantum interference device (SQUID). In the presence of an in-plane magnetic field, obvious magnetic hysteresis loops were observed at both 10 and 300 K, providing direct evidence for the ferromagnetism of the exfoliated VSe_2 sample (**Figure 4**a). The *M*–*H* curves of VSe_2 bulk crystal and SiO_2 substrate were also investigated to eliminate the contribution of substrate and bulk crystal, which were determined to be paramagnetic and diamagnetic, respectively (Figure S7a,b, Supporting Information). The temperature-dependent saturated magnetization (M_s) of VSe_2 in Figure 4b indicates a high T_c up to 470 K, which is much higher than that observed in other exfoliated 2D

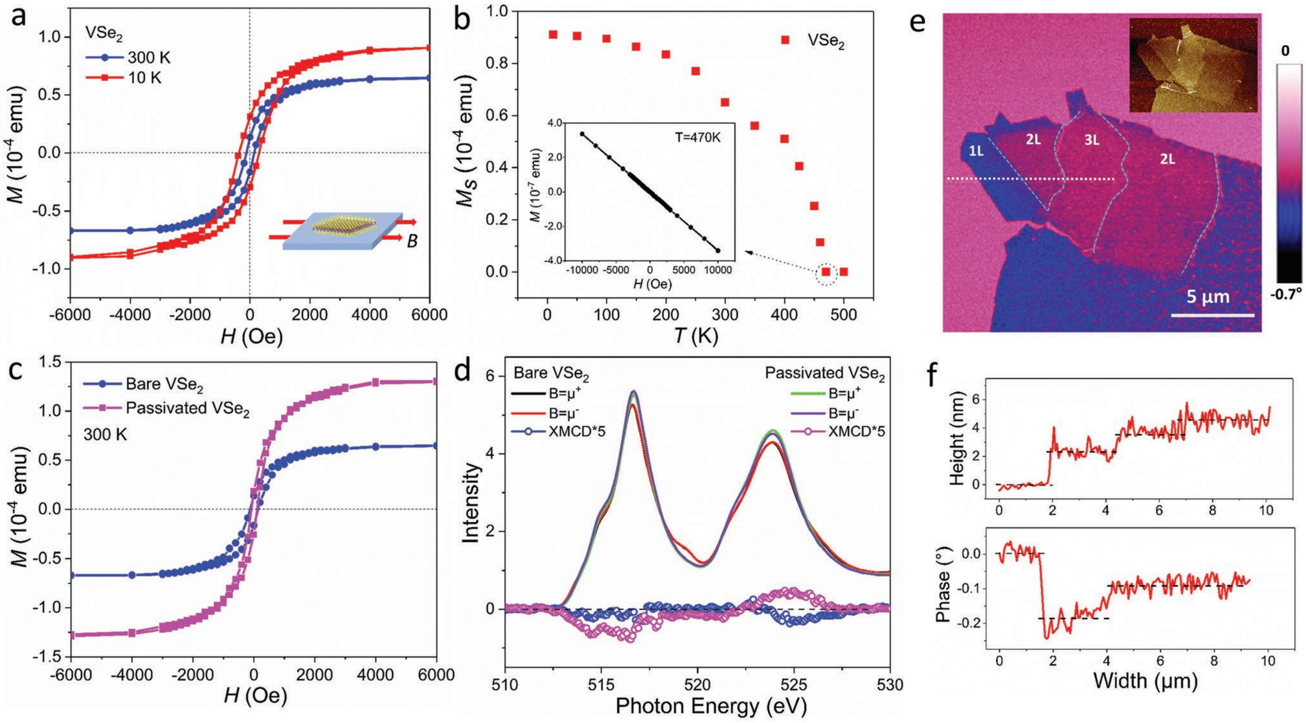

Figure 4. Ferromagnetism of exfoliated VSe_2 flakes. a) *M*–*H* hysteresis loop of bare VSe_2 flakes on SiO_2 substrate under an in-plane magnetic field at 300 and 10 K. b) Temperature-dependent saturated magnetization (M_s) of bare VSe_2 from 10 to 500 K. Inset: *M*–*H* curve for the sample at 470 K indicating the loose of magnetization. c) *M*–*H* hysteresis loop of bare and passivated VSe_2 flakes at 300 K. d) XMCD spectra on V L-edge of bare and passivated VSe_2 flakes on HOPG substrate at room temperature (μH = ±2 T). e) MFM phase image of a passivated VSe_2 monolayer/bilayer/trilayer flake, the MFM signal is reflected from the phase color bar increasing from red to blue. Inset: 3D topography image. f) Topography height and MFM phase profiles of the MFM image corresponding to the white dashed line in panel (e).

ferromagnets, including CrI_3, $Cr_2Ge_2Te_6$, and Fe_3GeTe_2. Meanwhile, the zero-field cooling magnetization presents a significant jump at around 130 K corresponding to a CDW transition temperature (T_{CDW}) of the VSe_2 ultrathin flakes, which is consistent with the values reported on MBE monolayer exfoliated thin VSe_2 (Figure S7c, Supporting Information).[8,30]

Monolayer VSe_2 is highly unstable in the air and is easily oxidized to vanadium oxides (V_2O_5) which is a diamagnetic insulator at room temperature.[31] To minimize the degradation effect, the magnetization of the chemically passivated VSe_2 was also investigated using SQUID at 300 K. Due to uncertainty in the mass of monolayer flakes, the values reported here are nominal values and sample amounts are kept as the same by volume of solution to achieve reliable comparison of magnetizations. A much enhanced M_s of 1.3×10^{-4} emu was obtained for the passivated samples as compared to bare sample (0.7×10^{-4} emu) at a similar coercive field (H_c) (≈120 Oe) (Figure 4c). Element-specific X-ray magnetic circular dichroism (XMCD) was also conducted to further demonstrate the passivation enhanced ferromagnetism of the exfoliated VSe_2 (Figure 4d). The V L-edge of VSe_2 was investigated under room temperature with two opposite directions of horizontal magnetic fields relative to the fixed photon helicity of μ^+ and μ^- ($\mu H = \pm 2$ T), and the difference of $\mu^+ - \mu^-$ is defined as the XMCD signal. There are clear XMCD signals ($\mu^+ - \mu^-$ is nonzero) for both bare and passivated VSe_2 samples, supporting the evidences of room-temperature ferromagnetism on VSe_2 flakes, and the intensity enhanced significantly after chemical passivation, where the total magnetic moment (spin and orbital magnetic moments) increased from 0.094 μ_B to 0.315 μ_B per V atom.[32] The measured magnetic moment of the chemically passivated flakes is in the same order as that theoretically predicted for 1T-VSe_2 monolayer (≈0.10 μ_B).[9–11] We are aware there are a few reports on MBE grown VSe_2 film where no exchange splitting was observed in ARPES, thus revealing the absence of ferromagnetism.[15,18,19] These VSe_2 samples were grown by MBE on polycrystalline HOPG, thus the film inevitably contained a lot of grain boundaries and rotationally disordered domains, which would lead to spin frustration. In contrast, our exfoliated VSe_2 monolayers are large size single crystal domains peeled from high quality VSe_2 crystal and randomly distributed on a substrate (see Figure 1c).

The air-stability of the passivated VSe_2 flakes makes it possible to study the magnetic properties of individual flake using ambient magnetic force microscopy (MFM); this is rarely performed on 2D ferromagnetic materials due to their extreme air instability. As opposed to SQUID or XMCD measurements that only give an average signal, MFM provides spatially resolved magnetic signal that allows us to correlate the ferromagnetic signal with the layer thickness. As shown in Figure 4e,f, passivated monolayer (2.3 nm), bilayer (3.4 nm), and trilayer (4.4 nm) VSe_2 flakes, were investigated. Their height differences can be distinguished from the stepped height profile in Figure 4f (top) corresponding to the white dash line in Figure 4e and the inserted 3D topography image in Figure 4e. From the MFM phase image, it is obvious that the monolayer exhibits a much higher magnetic signal (larger phase contrast) compared to thicker flakes. The MFM phase profile in Figure 4f (bottom) reveals that the monolayer (–0.18°) shows more than double the phase shift of bilayer and trilayer (–0.08°). This result is consistent with previously reported thickness-dependent ferromagnetism on MBE grown VSe_2 samples.[8]

In previous studies on the ferromagnetism of 2D VSe_2, the role of atomic vacancies was ignored. Here, a systematic investigation on the correlation between Se vacancy and magnetization was performed. First, Se vacancies were generated in VSe_2 sample by thermally annealing in UHV (600 °C, overnight). The M–H hysteresis loops of VSe_2 before and after thermal annealing is presented in **Figure 5**a, where a remarkably enhanced ferromagnetism over that of the intrinsic baseline level is observed. The reduced intensity of the XPS Se3d spectra (normalized by the intensity of V2p spectra) for the thermally annealed sample indicates an increased Se vacancy concentration with Se/V ratio decreased from 1.83 to 1.76 (Figure 5a, inset). Exfoliated ultrathin VSe_2 flakes undergo slow degradation in PC solvent, leading to the formation of Se vacancies. AFM topography images reveal increasing defect concentration with time; this has also been verified by XPS analysis, indicating a decreased Se/V ratio from 1.83 to 1.72 (Figure S8a,b, Supporting Information). Corresponding ferromagnetic intensities were monitored by SQUID at 300 K and the M_s value shows an increased intensity from 0.9×10^{-4} to 1.8×10^{-4} emu, indicating Se vacancy enhances ferromagnetism (Figure 5b, red curve and Figure S8c, Supporting Information). The correlation of Se vacancy and magnetic moment of monolayer VSe_2 has also been studied using density functional theory (DFT) calculation. A similar rising trend of magnetic moment with increasing vacancy concentrations is obtained (Figure 5b, purple curve). The magnetic moment of intact VSe_2 monolayer (Se/V = 2.0) from our DFT calculation is around 1.2 μ_B per V atom, which is consistent with previous calculation results indicating intrinsic ferromagnetism.[11] We have also calculated the trend under different Hubbard U values, a similar trend of increasing magnetic moments with Se vacancy concentrations is predicted (Figure S9, Supporting Information). In addition, DFT calculations reveal that the adsorption of O_2 or thiol molecules on the Se vacancies decrease the magnetizations of VSe_2 monolayer to near the intrinsic level due to the consumption of unpaired electrons for V around Se vacancies (Figure 5c). It suggests that although defects can contribute to ferromagnetism, they are not robust in air. Moreover, thiol adsorption shows higher magnetization than O_2 that agrees well with above SQUID and XMCD results of passivation enhanced magnetism, demonstrating the protection effect on Se vacancies against air O_2. Thus thiol passivation can reduce defect-induced magnetization without affecting intrinsic ferromagnetism, and its presence is in fact necessary to prevent air-induced degradation of the samples.

Although the measured magnetism from our exfoliated VSe_2 material most probably has mixed contributions from both intrinsic and defect-related ferromagnetism, DFT calcuations show that passivation by thiol molecules on Se vacancy sites should quench defect-related magentism. The fact that we managed to observe robust ferromagnetism most strongly on thiol-passivated monolayer flakes suggest that the intrinsic ferromagnetism provides the lower limit of the observed ferromagnetism, while increasing defect concentration will increase it to the upper limit.

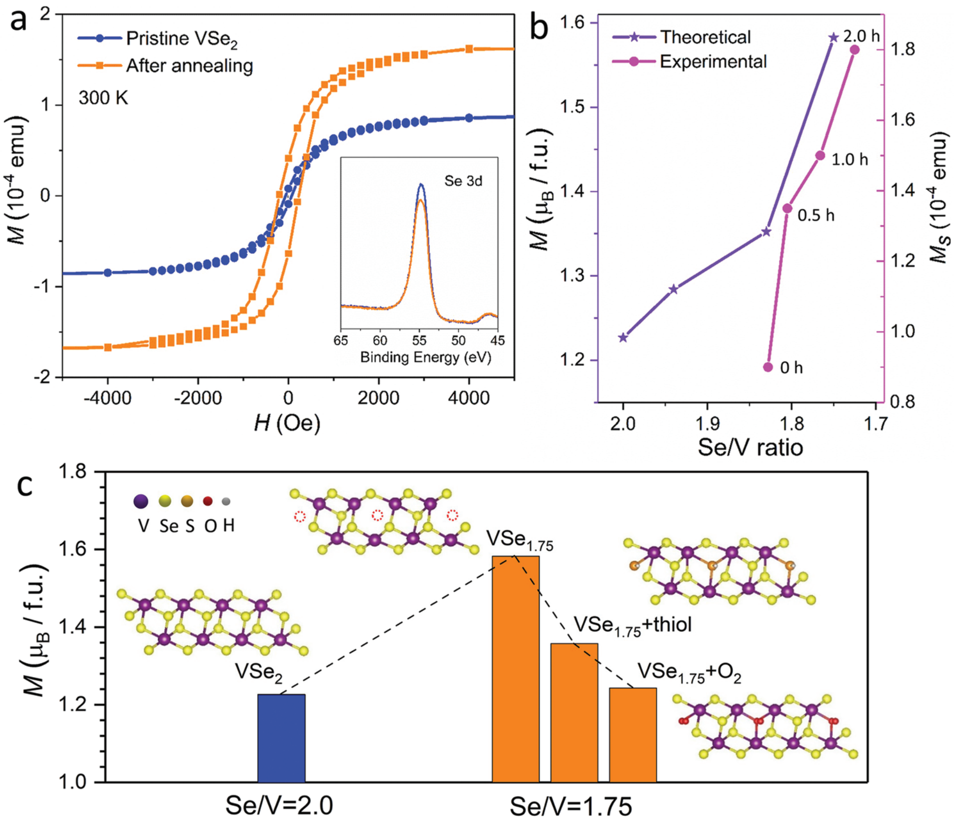

Figure 5. Se vacancy enhanced ferromagnetism of exfoliated VSe_2 flakes. a) *M–H* curves of pristine and thermal annealed VSe_2 samples. Inset: the corresponding XPS Se3d spectra after normalization by V2p spectra, indicating the increased Se vacancies after thermal annealing. b) The variation trends of theoretical (purple) and experimental (red) magnetization versus Se/V ratio of increasing vacancy concentrations produced by increasing the chemical degradation time in solution. c) Theoretically calculated magnetizations of intact (VSe_2), defective ($VSe_{1.75}$), thiol ($VSe_{1.75}$+thiol), and oxygen ($VSe_{1.75}+O_2$) adsorbed monolayer VSe_2, and their corresponding atomic structures.

By performing electrochemical exfoliation of VSe_2 crystal using organic intercalants, large sized ultrathin 1T-VSe_2 flakes with thickness fewer than five layers can be obtained with >90% yield, of which the monolayer flakes dominate (43%). Using a combination of SQUID, XMCD, and MFM, we confirmed the presence of room-temperature ferromagnetism in monolayer 1T-VSe_2 flakes with a magnetic moment ≈0.3 μ_B per V atom as determined by XMCD. Although we are not able to conclude if all the measured magnetic signals are intrinsic in nature, both our experimental and computational results confirm that the presence of Se vacancies can enhance the measured signal, thus claims of intrinsic ferromagnetism in VSe_2 has to be qualified by generating a defect-free sample.

Supporting Information

Supporting Information is available from the Wiley Online Library or from the author.

Acknowledgements

W.Y. and J.L. contributed equally to this work. K.P.L. thanks MOE Tier 3 grant 2D crystal quantum exciton photonics MOE2018-T3-1-005. This work was supported by the Agency for Science and Technology, Singapore, AME-IRG funding under the project "Scalable Growth of Ultrathin Ferroelectric Materials for Memory Technologies (A1983c0035)." The authors thank Dr. Fangfang Zhao at Bruker Singapore Pte. Ltd. for the MFM measurements.

Conflict of Interest

The authors declare no conflict of interest.

Keywords

2D ferromagnetism, chemical exfoliation, covalent passivation, vacancy enhanced ferromagnetism, VSe_2 monolayers

Received: June 14, 2019
Revised: July 26, 2019

---

[1] N. Samarth, *Nature* **2017**, *546*, 216.
[2] C. Gong, X. Zhang, *Science* **2019**, *363*, 6428.
[3] K. S. Burch, D. Mandrus, J. G. Park, *Nature* **2018**, *563*, 7729.
[4] N. D. Mermin, H. Wagner, *Phys. Rev. Lett.* **1966**, *17*, 1133.

[5] B. Huang, G. Clark, E. Navarro-Moratalla, D. R. Klein, R. Cheng, K. L. Seyler, D. Zhong, E. Schmidgall, M. A. McGuire, D. H. Cobden, W. Yao, *Nature* **2017**, *546*, 270.
[6] C. Gong, L. Li, Z. Li, H. Ji, A. Stern, Y. Xia, T. Cao, W. Bao, C. Wang, Y. Wang, Z. Q. Qiu, *Nature* **2017**, *546*, 265.
[7] Z. Fei, B. Huang, P. Malinowski, W. Wang, T. Song, J. Sanchez, W. Yao, D. Xiao, X. Zhu, A. F. May, W. Wu, *Nat. Mater.* **2018**, *17*, 778.
[8] M. Bonilla, S. Kolekar, Y. Ma, H. C. Diaz, V. Kalappattil, R. Das, T. Eggers, H. R. Gutierrez, M. H. Phan, M. Batzill, *Nat. Nanotechnol.* **2018**, *13*, 289.
[9] Y. Ma, Y. Dai, M. Guo, C. Niu, Y. Zhu, B. Huang, *ACS Nano* **2012**, *6*, 1695.
[10] F. Li, K. Tu, Z. Chen, *J. Phys. Chem. C* **2014**, *118*, 21264.
[11] Z. I. Popov, N. S. Mikhaleva, M. A. Visotin, A. A. Kuzubov, S. Entani, H. Naramoto, S. Sakai, P. B. Sorokin, P. V. Avramov, *Phys. Chem. Chem. Phys.* **2016**, *18*, 33047.
[12] H. R. Fuh, B. Yan, S. C. Wu, C. Felser, C. R. Chang, *New J. Phys.* **2016**, *18*, 113038.
[13] E. Marco, R. G. Hennig, D. C. Johnson, *Phys. Rev. B* **2017**, *96*, 235147.
[14] J. Yang, W. Wang, Y. Liu, H. Du, W. Ning, G. Zheng, C. Jin, Y. Han, N. Wang, Z. Yang, M. Tian, *Appl. Phys. Lett.* **2014**, *105*, 063109.
[15] G. Duvjir, B. K. Choi, I. Jang, S. Ulstrup, S. Kang, T. Thi Ly, S. Kim, Y. H. Choi, C. Jozwiak, A. Bostwick, E. Rotenberg, *Nano Lett.* **2018**, *18*, 5432.
[16] W. Y. Tong, S. J. Gong, X. Wan, C. G. Duan, *Nat. Commun.* **2016**, *7*, 13612.
[17] P. Coelho, K. Nguyen-Cong, M. Bonilla, S. K. Kolekar, M. H. Phan, J. Avila, M. C. Asensio, I. I. Oleynik, M. Batzill, *J. Phys. Chem. C* **2019**, *123*, 14089.
[18] J. Feng, D. Biswas, A. Rajan, M. D. Watson, F. Mazzola, O. J. Clark, K. Underwood, I. Markovic, M. McLaren, A. Hunter, D. M. Burn, *Nano Lett.* **2018**, *18*, 4493.
[19] P. K. J. Wong, W. Zhang, F. Bussolotti, X. Yin, T. S. Herng, L. Zhang, Y. L. Huang, G. Vinai, S. Krishnamurthi, D. W. Bukhvalov, Y. J. Zheng, *Adv. Mater.* **2019**, *18*, 1901185.
[20] C. Wang, Q. He, U. Halim, Y. Liu, E. Zhu, Z. Lin, H. Xiao, X. Duan, Z. Feng, R. Cheng, N. O. Weiss, *Nature* **2018**, *555*, 231.
[21] J. Li, C. Chen, S. Liu, J. Lu, W. P. Goh, H. Fang, Z. Qiu, B. Tian, Z. Chen, C. Yao, W. Liu, *Chem. Mater.* **2018**, *30*, 2742.
[22] S. Yang, K. Zhang, A. G. Ricciardulli, P. Zhang, Z. Liao, M. R. Lohe, E. Zschech, P. W. Blom, W. Pisula, K. Müllen, X. Feng, *Angew. Chem., Int. Ed.* **2018**, *130*, 4767.
[23] D. Hanlon, C. Backes, E. Doherty, C. S. Cucinotta, N. C. Berner, C. Boland, K. Lee, A. Harvey, P. Lynch, Z. Gholamvand, S. Zhang, *Nat. Commun.* **2015**, *6*, 8563.
[24] M. Esters, R. G. Hennig, D. C. Johnson, *Phys. Rev. B* **2017**, *96*, 235147.
[25] Z. Zhang, J. Niu, P. Yang, Y. Gong, Q. Ji, J. Shi, Q. Fang, S. Jiang, H. Li, X. Zhou, L. Gu, *Adv. Mater.* **2017**, *29*, 1702359.
[26] H. Li, Q. Zhang, C. C. R. Yap, B. K. Tay, T. H. T. Edwin, A. Olivier, D. Baillargeat, *Adv. Funct. Mater.* **2012**, *22*, 1385.
[27] S. S. Chou, M. De, J. Kim, S. Byun, C. Dykstra, J. Yu, J. Huang, V. P. Dravid, *J. Am. Chem. Soc.* **2013**, *135*, 4584.
[28] E. P. Nguyen, B. J. Carey, J. Z. Ou, J. van Embden, E. D. Gaspera, A. F. Chrimes, J. Spencer, S. M. Zhuiykov, K. Kalantar-zadeh, T. Daeneke, *Adv. Mater.* **2015**, *27*, 6225.
[29] D. M. Sim, M. Kim, S. Yim, M. J. Choi, J. Choi, S. Yoo, Y. S. Jung, *ACS Nano* **2015**, *9*, 12115.
[30] Á. Pásztor, A. Scarfato, C. Barreteau, E. Giannini, C. Renner, *2D Mater.* **2017**, *4*, 041005.
[31] Z. R. Xiao, G. Y. Guo, P. H. Lee, H. S. Hsu, J. C. A. Huang, *J. Phys. Soc. Jpn.* **2008**, *77*, 023706.
[32] C. T. Chen, Y. U. Idzerda, H. J. Lin, N. V. Smith, G. Meigs, E. Chaban, G. H. Ho, E. Pellegrin, F. Sette, *Phys. Rev. Lett.* **1995**, *75*, 152.